EXTENDED PDF FORMAT
SPONSORED BY
usb
www.usbweb.com

Science
AAAS

Widespread Morning Drizzle on Titan

Máté Ádámkovics, *et al.*

Science **318**, 962 (2007);
DOI: 10.1126/science.1146244

The following resources related to this article are available online at www.sciencemag.org (this information is current as of November 14, 2007):

Updated information and services, including high-resolution figures, can be found in the online version of this article at:
http://www.sciencemag.org/cgi/content/full/318/5852/962

Supporting Online Material can be found at:
http://www.sciencemag.org/cgi/content/full/1146244/DC1

This article **cites 23 articles**, 5 of which can be accessed for free:
http://www.sciencemag.org/cgi/content/full/318/5852/962#otherarticles

This article appears in the following **subject collections**:
Planetary Science
http://www.sciencemag.org/cgi/collection/planet_sci

Information about obtaining **reprints** of this article or about obtaining **permission to reproduce this article** in whole or in part can be found at:
http://www.sciencemag.org/about/permissions.dtl

Downloaded from www.sciencemag.org on November 14, 2007

Science (print ISSN 0036-8075; online ISSN 1095-9203) is published weekly, except the last week in December, by the American Association for the Advancement of Science, 1200 New York Avenue NW, Washington, DC 20005. Copyright 2007 by the American Association for the Advancement of Science; all rights reserved. The title *Science* is a registered trademark of AAAS.

2. Yu. N. Osetsky, D. J. Bacon, *Nucl. Instrum. Methods Phys. Res. B* **180**, 85 (2001).
3. A. J. E. Foreman, C. A. English, W. J. Phythian, *Philos. Mag. A* **66**, 655 (1992).
4. Yu. N. Osetsky, D. J. Bacon, A. Serra, B. N. Singh, S. I. Golubov, *Philos. Mag.* **83**, 61 (2003).
5. J. Marian *et al.*, *Phys. Rev. B* **65**, 144102 (2002).
6. E. Kuramoto, *J. Nucl. Mater.* **276**, 143 (2000).
7. B. D. Wirth, G. R. Odette, D. Maroudas, G. E. Lucas, *J. Nucl. Mater.* **276**, 33 (2000).
8. S. L. Dudarev, *Philos. Mag.* **83**, 3577 (2003).
9. H. Trinkaus, B. N. Singh, A. J. E. Foreman, *J. Nucl. Mater.* **206**, 200 (1993).
10. F. Seitz, *Phys. Rev.* **79**, 723 (1950).
11. K. Arakawa, M. Hatanaka, E. Kuramoto, K. Ono, H. Mori, *Phys. Rev. Lett.* **96**, 125506 (2006).
12. M. Kiritani, *J. Nucl. Mater.* **251**, 237 (1997).
13. T. Hayashi, K. Fukumoto, H. Matsui, *J. Nucl. Mater.* **307–311**, 993 (2002).
14. H. Abe, N. Sekimura, Y. Yang, *J. Nucl. Mater.* **323**, 220 (2003).
15. K. Ohsawa, E. Kuramoto, *Phys. Rev. B* **72**, 054105 (2005).
16. The crowdions located at the loop center have a smaller energy barrier for motion than that of the crowdions located on the loop perimeter (*4*). This is because the most stable configuration for single SIAs is the dumbbell: The crowdions on the loop perimeter are more likely to transform to dumbbell configuration. Conversely, Marian (*5*) claimed that crowdion jumps are more likely to occur at the loop perimeter. This is because the interatomic potential used by Marian incorrectly predicts the crowdion configuration to be more stable than the dumbbell configuration.
17. Yu. N. Osetsky, D. J. Bacon, A. Serra, *Philos. Mag. Lett.* **79**, 273 (1999).
18. J. P. Hirth, J. Lothe, *Theory of Dislocations* (McGraw-Hill, New York, ed. 2, 1982).
19. M. Kiritani *et al.*, *Philos. Mag. Lett.* **79**, 797 (1999).
20. S. Kojima *et al.*, *Philos. Mag. A* **59**, 519 (1989).
21. N. M. Ghoniem, D. Walgraef, S. J. Zinkle, *J. Computer-Aided Mater. Des.* **8**, 1 (2002).
22. A. Seeger, N. Y. Jin, F. Phillip, M. Zaiser, *Ultramicroscopy* **39**, 342 (1991).
23. C. Tölg, P. Hähner, M. Zaiser, W. Frank, *Appl. Phys. A* **58**, 3 (1994).
24. D. Kuhlmann-Wilsdorf, *Acta Metall.* **13**, 257 (1965).
25. J. E. Bauerle, J. S. Koehler, *Phys. Rev.* **107**, 1493 (1957).
26. M. Kiritani, *J. Phys. Soc. Jpn.* **40**, 1035 (1976).
27. We did not regard the loop migration of 15 nm as a ballistic jump because of the following context. The 1D migration of dislocation loop is a result of collective motion of numerous atoms whose elementary jump length is d_{110}, the interplanar distance between (110) planes. Although the vacancy loop migrated ballistically 15 nm within a few video frames, it seems reasonable to assume that this migration consists of several hundred jumps of a few hundred atoms in the same direction, involving thermally activated atomic jumps in the reverse direction on an atomic scale.
28. The loop shape (triangle or circular) is unidentifiable in the edge-on view.
29. S. B. Fisher, *Radiat. Eff.* **5**, 239 (1970).

30. This research was sponsored by the Office of Fusion Energy Sciences, U.S. Department of Energy. The microscope facility within the SHaRE (Shared Research Equipment User Facility) Collaborative Research Center at ORNL was supported by the Division of Scientific User Facilities, Office of Basic Energy Science. We are grateful to Y. N. Osetsky, S. I. Golubov, B. N. Singh, and P. J. Kamenski for valuable comments.

Supporting Online Material
www.sciencemag.org/cgi/content/full/318/5852/959/DC1
Materials and Methods
SOM Text
Figs. S1 to S4
Movies S1 to S3

25 July 2007; accepted 3 October 2007
10.1126/science.1148336

Widespread Morning Drizzle on Titan

Máté Ádámkovics,[1,2]* Michael H. Wong,[1] Conor Laver,[1] Imke de Pater[1,2]

Precipitation is expected in Titan's atmosphere, yet it has not been directly observed, and the geographical regions where rain occurs are unknown. Here we present near-infrared spectra from the Very Large Telescope and W. M. Keck Observatories that reveal an enhancement of opacity in Titan's troposphere on the morning side of the leading hemisphere. Retrieved extinction profiles are consistent with condensed methane in clouds at an altitude near 30 kilometers and concomitant methane drizzle below. The moisture encompasses the equatorial region over Titan's brightest continent, Xanadu. Diurnal temperature gradients that cause variations in methane relative humidity, winds, and topography may each be a contributing factor to the condensation mechanism. The clouds and precipitation are optically thin at 2.0 micrometers, and models of "subvisible" clouds suggest that the droplets are 0.1 millimeter or larger.

A zoo of clouds is scattered across Saturn's largest moon, Titan, including convective clouds near the south pole (*1*, *2*), geographically controlled clouds at 40°S latitude (*3*), and a large cloud of ethane near the north pole (*4*). These and other types of clouds have been predicted with the use of combinations of chemical, microphysical, and general circulation models (*5*, *6*). Analysis of the methane relative humidity profile at the Huygens probe entry site suggests that there is a solid-methane cloud from 20 to 30 km altitude and a light drizzle of methane that wets the surface (*7*). However, the fluvial channels seen at the landing site (*8*) are due to heavier rainfall (*9*), which may occur during intense storms that are predicted by dynamical models (*10*). Conditions in the lower troposphere are best constrained where the Huygens probe landed, yet a single weather station cannot characterize Titan's meteorology on a planetwide scale. If widespread, methane condensation could be the dominant pathway for returning methane to the surface and closing the methane cycle.

Because the near-infrared aerosol opacity τ in Titan's atmosphere is low ($\tau = 0.2$ at 2 μm), light can penetrate to the surface at wavelengths where methane absorption is negligible (*11*). Radiative transfer (RT) models of Titan's spectra have been used to probe the heights of cloud tops and the aerosol vertical structure (*1*, *2*, *12*, *13*). One of the main challenges in accurately retrieving altitudes with these models is that the contribution function for a particular wavelength is dependent on the vertical distribution of aerosol. Variations in surface reflectivity can also be masked by near-surface atmospheric opacity. One way to break these degeneracies is to simultaneously analyze spectra taken along different paths through the atmosphere. Spatially resolved spectra from a new class of instruments, such as the OH-Suppressing InfraRed Imaging Spectrograph (OSIRIS) (*14*) at the W. M. Keck Observatory or the Spectrograph for INtegral Field Observations in the Near Infrared (SINFONI) (*15*) at the Very Large Telescope (VLT), are an ideal source of data for such an analysis. These instruments may be used to create a global picture of Titan's lower atmosphere and surface.

During our campaign to monitor the seasonal changes in the global distribution of Titan's aerosol, we observed Titan on 28 February 2005 universal time (UT) with SINFONI (*13*) and on 17 April 2006 UT with OSIRIS. Together the two instruments provide independent measurements of Titan at different epochs and viewing geometries. Systematic errors that arise from mosaicking and correcting for Earth's atmosphere (fig. S1) are specific to each instrument, and comparison facilitates the rejection of observational artifacts. Here we describe a method for making measurements of condensed-phase opacity from specific altitude regions in Titan's atmosphere using narrow (10- to 15-nm) spectral bandpass difference imaging. We used RT models to quantify the altitude and magnitude of the opacity enhancements, and we report the detection of widespread methane drizzle: precipitation from stratiform clouds of solid methane.

In order to discern the light scattered by clouds, drizzle, and haze in the lower troposphere, the contribution from the surface albedo variation (Fig. 1A) was removed from the images that probed the bottom of the atmosphere (Fig. 1B). We empirically quantified the relative surface flux f in images taken at wavelengths with significant and with negligible methane gas opacity by minimizing the correlation coefficient between the surface-subtracted image of the atmosphere and the image of the surface (fig. S2). The mean surface flux in images probing the lower troposphere is ~72% of the flux in images of the surface, which is confirmed by our RT models. After subtracting the surface contribution from images that probe the lower troposphere, we can identify equatorial opacity changes

[1]Department of Astronomy, University of California, Berkeley, CA 94611, USA. [2]Center for Integrative Planetary Science, University of California, Berkeley, CA 94611, USA.

*To whom correspondence should be addressed. E-mail: mate@berkeley.edu

Downloaded from www.sciencemag.org on November 14, 2007

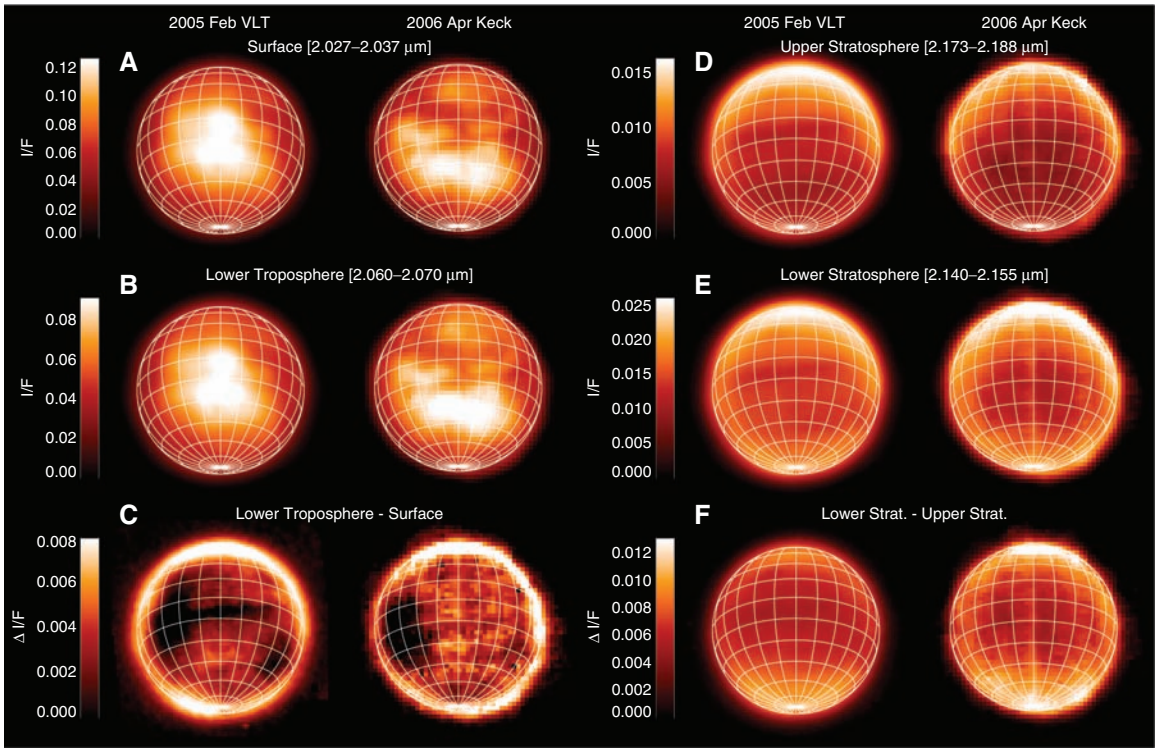

Fig. 1. Difference imaging of the condensed-phase scattering at specific altitudes in the atmosphere. The lower troposphere (below 20 km) can be probed by subtracting images at wavelengths sensitive to the variations in surface reflectivity (**A**) from those that probe both the surface and the lower troposphere (**B**). The difference images (**C**) reveal a dark feature in the morning equatorial regions, with sub-observer longitudes of 89°W and 42°W for the VLT and Keck, respectively. Artifacts such as the narrow linear feature in the VLT data are not observed with both instruments. The regions with lower $\Delta I/F$ in the difference images (C) have increased atmospheric opacity. The lower stratosphere can be similarly probed by subtracting images of the upper stratosphere (**D**) from images of the lower stratosphere (**E**) to highlight the contrast from the SPH (**F**); in this case, larger $\Delta I/F$ indicates more scattering. Difference images of the troposphere and stratosphere have a (1σ) pixel-to-pixel noise of $\Delta I/F$ = 0.003 and 0.0005, respectively.

on the morning (left) side of the disk in both observations (Fig. 1C). The dark regions cover slightly different portions of the disk because of different viewing angles during the two observations, yet correspond to the same latitudes on Titan, so the observation of the dark feature in both data sets is a confirmation of the localized change in opacity.

The nature of the increased opacity is determined by creating a model of the observed datacube. A 1.50- to 2.25-μm spectrum, corresponding to each observed spatial pixel, was calculated using a two-stream numerical solution to the RT equation (*16*, *17*). We accounted for the spatial variation in surface albedo by using a Visual and Infrared Mapping Spectrometer (VIMS) map of the 2.018-μm albedo (*18*) as input for the surface reflectivity. The surface spectrum is gray with four Gaussian absorption features (*19*). The aerosol (haze) extinction at the tropopause is 0.0025 km^{-1} at southern latitudes above 45°S and increases toward the north by a factor of 0.0065 per degree of latitude (*13*). Aerosol extinction decreases with altitude above the tropopause, with a scale height of 100 km. The south polar hood (SPH) is included as a doubling of extinction from 50 to 70 km altitude and is located poleward of 45°S. Uniform aerosol extinction (0.001 km^{-1}), consistent with results from the Huygens probe, was used throughout the troposphere. Based on the temperature at a particular altitude, condensed-phase methane opacity was included as a layer of liquid or solid methane. The optical depth of condensed methane is the product of the absorption coefficient (*20*) and path length (i.e., column volume). A normalized point spread function from a calibration star was used to convolve the model for comparison with the observations. Images from the model datacube show excellent agreement with the observed data (fig. S1).

Fig. 2. Contrast in the difference images (Fig. 1, C and F) is due to localized changes in extinction. In order to understand that the dark region in Fig. 1C is due to a relative increase in opacity, we calculated the expected contrast in the lower troposphere (solid line) and lower stratosphere (dotted line).

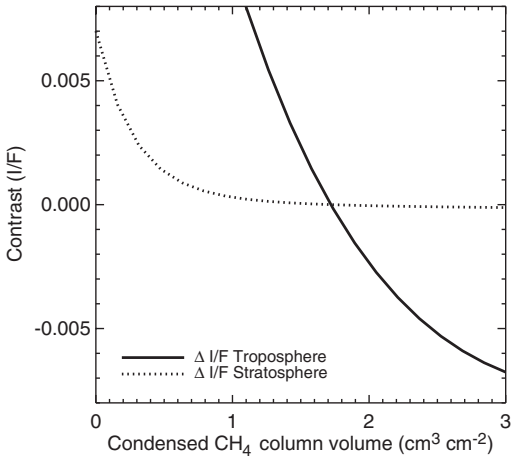

With a model of Titan's atmosphere and surface, various hypotheses for the source of the observed dark contrast feature (Fig. 1C) may be tested. We calculated a characteristic spectrum and determined the mean flux in the wavelength regions corresponding to images in Fig. 1 to obtain a nominal subtracted image flux ($\Delta I/F_0$) for both the lower troposphere and the lower stratosphere. The contrast was then defined as the difference between $\Delta I/F_0$ and the $\Delta I/F$ from a new spectrum in which a model parameter was changed. In Fig. 2, we plot the contrast expected in images of the lower troposphere and lower stratosphere when the column of condensed-phase methane is varied. Changes in aerosol haze density have been systematically ruled out by inadequately reproducing the observed contrast. If the observed opacity enhancement were attributed to small tropospheric haze particles (<0.001 mm), then the steep wavelength dependence of the extinction efficiency would extrapolate to unit optical depth at 0.938 μm (fig. S3), yet there have not been reports of aerosol enhancements over Xanadu or near the morning hemisphere. On the other hand, a mist

Downloaded from www.sciencemag.org on November 14, 2007

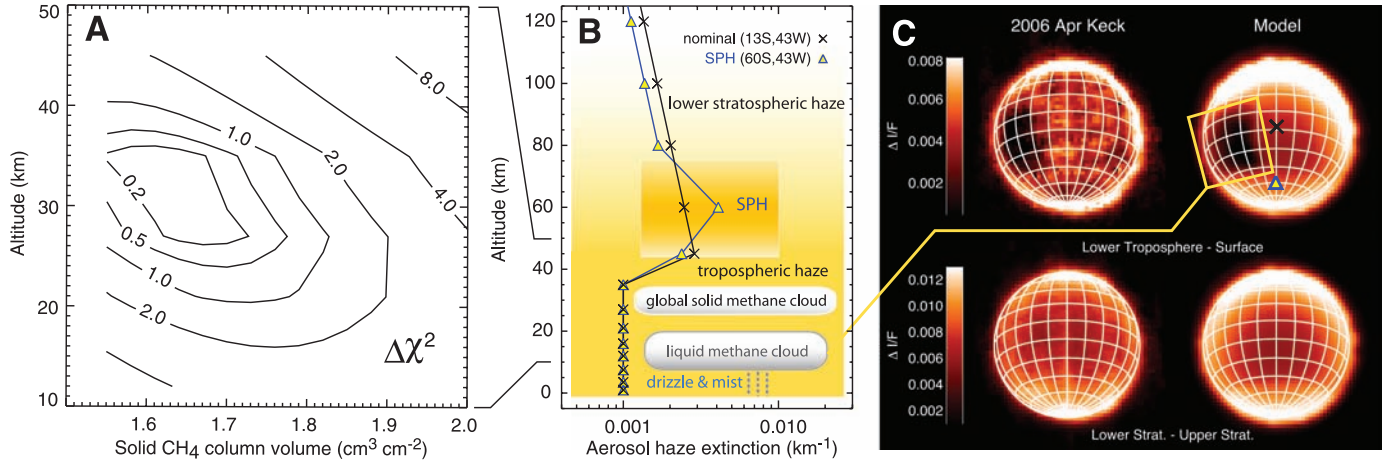

Fig. 3. A disk-encompassing cloud of condensed-phase methane is revealed by goodness-of-fit ($\Delta\chi^2$) contours for several altitudes and column volumes of methane (**A**). Vertical profiles of 2-μm aerosol extinction at two locations on the disk along with altitudes of condensed methane clouds show the altitudes of large-scale atmospheric features (**B**). Difference images extracted from the RT model of the observed OSIRIS datacube quantitatively reproduce the contrast caused by the enhancement in lower tropospheric opacity and the south polar hood (SPH) (**C**). Extinction profiles from the center of the disk (black crosses) and from the SPH (blue triangles) show the characteristic differences in the aerosol densities at south and equatorial latitudes.

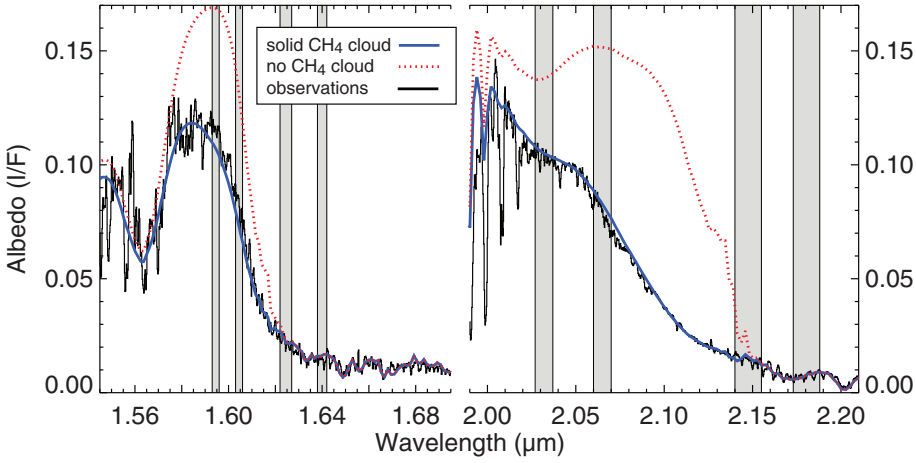

Fig. 4. Opacity caused by a cloud of solid methane provides a significantly improved fit of spectra at all locations on the disk. A representative Keck/OSIRIS spectrum from the center of the disk (black) is compared against model spectra with (blue) and without (red) a cloud of solid methane in the 25- to 30-km layer of the model. Shaded vertical regions indicate spectral bandpasses used for difference imaging in Fig. 1 and fig. S5.

or drizzle of methane droplets (>0.01 mm) that is optically thin at 2.0 μm would be optically thin at visible wavelengths as well and could more easily elude detection.

The altitude and total column of condensed methane were fit to observations by minimizing the root mean square deviation between a model datacube and observations. The cloud of methane was indeed found to be globally widespread, with a column volume of 1.65 $cm^3\ cm^{-2}$ in the altitude range of 25 to 35 km (Fig. 3A). Temperatures at these altitudes indicate that methane must be a solid (*7*). The morning enhancement of opacity is consistent with an additional column volume of 0.25 $cm^3\ cm^{-2}$ below 20 km, where methane is a liquid (Fig. 3B). The difference images are a sensitive test of the vertical profile of the tropospheric extinction, and the calculated datacubes with condensed methane opacity reproduce the observations (Fig. 3C). Artifacts or variations in surface absorption were are excluded by performing analogous (fig. S4) difference imaging at 1.5 μm. The difference images in the H band (fig. S5) can be used to independently reach all the qualitative conclusions arising from the K-band analysis (fig. S6). The improvement in spectral fit across both bands, when condensed methane is included, is illustrated in Fig. 4.

Depending on size and composition, drizzle will either reach the surface or form a near-surface mist. Although no direct detection of drizzle has been reported by Huygens (*8*), the uniform methane mixing ratio below 6 km (*21*) is consistent with the evaporation of methane from droplets (*22*). We detected both the solid methane cloud at 25 to 35 km and morning drizzle below. It had been suggested that precipitation from subvisible clouds would reach the surface and close the methane cycle and that the drizzle could be occurring over nearly 60% of the globe (*7*). By measuring the global extent of methane cloud, we see here that the methane drizzle is indeed precipitation related to stratiform clouds and does cover a substantial fraction of Titan.

Drizzle is observed in the morning hemisphere, and we first consider a diurnal mechanism that facilitates condensation. Because the methane is saturated around 15 km (*7*) in the morning [Huygens landed at local true solar time (LTST) of 9:47 a.m.], a small overnight drop in temperature at this altitude could initiate droplet formation that would then lead to drizzle in the lower troposphere. During our observations, it seems it was drizzling on Titan until approximately 10:40 a.m. LTST (roughly 3 Earth days after sunrise), which is consistent with the Huygens results.

Geographic factors may affect circulation and control localized condensation. One possibility is that the observed drizzle is due to the cooling of air caused by advection. Large-scale winds may push a moist airmass upslope, thus cooling it and driving condensation. Observations of sand dunes have shown that prevailing easterlies blow toward the bright continent of Xanadu (*23*). If the bright region is indeed a topographical high, then a "coastal" drizzle may form and cover the landmass. The relationship between the drizzle and the bright reflectivity of Xanadu is unclear (*24*), and it is possible that the drizzle contributes to rinsing the bright surface of the dark deposited aerosol. Perhaps the combination of nighttime cooling and local microclimates together make for consistently misty mornings in Xanadu.

References and Notes

1. M. E. Brown, A. H. Bouchez, C. A. Griffith, *Nature* **420**, 795 (2002).
2. C. A. Griffith *et al.*, *Science* **310**, 474 (2005).

Downloaded from www.sciencemag.org on November 14, 2007

3. H. G. Roe, M. E. Brown, E. L. Schaller, A. H. Bouchez, C. A. Trujillo, *Science* **310**, 477 (2005).
4. C. A. Griffith *et al.*, *Science* **313**, 1620 (2006).
5. E. L. Barth, O. B. Toon, *Icarus* **182**, 230 (2006).
6. P. Rannou, F. Montmessin, F. Hourdin, S. Lebonnois, *Science* **311**, 201 (2006).
7. T. Tokano *et al.*, *Nature* **442**, 432 (2006).
8. M. G. Tomasko *et al.*, *Nature* **438**, 765 (2005).
9. J. T. Perron *et al.*, *J. Geophys. Res.* (*Planets*) **111**, 11001 (2006).
10. R. Hueso, A. Sánchez-Lavega, *Nature* **442**, 428 (2006).
11. C. A. Griffith, T. Owen, R. Wagener, *Icarus* **93**, 362 (1991).
12. M. Ádámkovics, I. de Pater, H. G. Roe, S. G. Gibbard, C. A. Griffith, *Geophys. Res. Lett.* **31**, L17S05 (2004).
13. M. Ádámkovics *et al.*, *J. Geophys. Res.* (*Planets*) **111**, 7 (2006).
14. J. E. Larkin *et al.*, *Proc. SPIE* **4841**, 1600 (2003).
15. F. Eisenhauer *et al.*, *Proc. SPIE* **4841**, 1548 (2003).
16. O. B. Toon, C. P. McKay, T. P. Ackerman, K. Santhanam, *J. Geophys. Res.* **94**, 16287 (1989).
17. C. P. McKay, J. B. Pollack, R. Courtin, *Icarus* **80**, 23 (1989).
18. J. W. Barnes *et al.*, *Icarus* **186**, 242 (2007).
19. Gaussian absorptions are fit to the entire disk by minimizing the sum squared residuals over the entire cube. The best-fit absorptions have central wavelengths of 1.505, 1.563, 1.614, and 2.028 μm; full width at half maximum of 0.052, 0.012, 0.010, and 0.021 μm; and peak absorptions of 99, 85, 80, and 16% of the surface reflectivity, respectively.
20. W. M. Grundy, B. Schmitt, E. Quirico, *Icarus* **155**, 486 (2002).
21. S. K. Atreya *et al.*, *Planet. Space Sci.* **54**, 1177 (2006).
22. T. Tokano, F. Ferri, G. Colombatti, T. Mäkinen, M. Fulchignoni, *J. Geophys. Res.* (*Planets*) **111**, 8007 (2006).
23. R. D. Lorenz *et al.*, *Science* **312**, 724 (2006).
24. C. A. Griffith, *Nature* **364**, 511 (1993).

25. This work was supported by NSF and the Technology Center for Adaptive Optics, managed by the University of California at Santa Cruz under cooperative agreement AST-9876783, NASA grant NNG05GH63G, and the Center for Integrative Planetary Science at the University of California at Berkeley. Data presented here were obtained at the W. M. Keck Observatory atop the sacred mountain of Mauna Kea and at the VLT operated by the European Southern Observatory.

Supporting Online Material
www.sciencemag.org/cgi/content/full/1146244/DC1
Observations and Methods
Figs. S1 to S6
References

8 June 2007; accepted 5 October 2007
Published online 11 October 2007;
10.1126/science.1146244
Include this information when citing this paper.

Facultative Mate Choice Drives Adaptive Hybridization

Karin S. Pfennig

Mating with another species (hybridization) is often maladaptive. Consequently, females typically avoid heterospecifics as mates. Contrary to these expectations, female spadefoot toads were more likely to choose heterospecific males when exposed to environmental conditions that favor hybridization. Indeed, those females with phenotypic characteristics for which hybridization is most favorable were most likely to switch from choosing conspecifics to heterospecifics. Moreover, environmentally dependent mate choice has evolved only in populations and species that risk engaging in, and can potentially benefit from, hybridization. Thus, when the benefits of mate choice vary, females may radically alter their mate selection in response to their own phenotype and their environment, even to the point of choosing males of other species.

Mating between species typically results in no, few, or poor-quality offspring (*1*). Consequently, females generally prefer to mate with males of their own species (*1*–*3*). When hybridization does occur, it is often ascribed to mistakes during, or constraints on, female mate choice (*4*–*7*). Yet, hybridization can sometimes be beneficial (*8*), and females might facultatively adjust their choice of conspecific versus heterospecific mates depending on the fitness consequences of hybridization (*9*–*12*). Such facultative switches in female mate choice may thereby mediate adaptive hybridization and could explain patterns of hybridization observed in many species (*8*).

Spadefoot toads, *Spea bombifrons* and *Spea multiplicata*, risk hybridizing where they cooccur in the southwestern United States across ~20% of *S. bombifrons'* range (*13*, *14*). Hybrid offspring are viable and can reproduce, albeit with reduced fertility: Hybrid males can be sterile (*15*) [although the frequency of sterility among hybrid males is unknown (*16*)], and female hybrids produce fewer eggs than pure-species females (*15*). Hybridization between these species has historically been spatially variable, with hybrid frequency ranging from 0 to 40% across populations (*14*). Hybridization is most common in small ponds that tend to be shallow and highly ephemeral, with *S. bombifrons* females hybridizing more often than *S. multiplicata* females (*14*).

These observed patterns of hybridization may be explained if *S. bombifrons* females can benefit from hybridization. Spadefoots breed in ephemeral pools (Fig. 1, A and B), and their tadpoles often fail to metamorphose before ponds dry (*17*). *S. multiplicata* develop more rapidly than *S. bombifrons*, and hybrid tadpoles metamorphose sooner than pure *S. bombifrons* tadpoles (*14*). Thus, for *S. bombifrons* females, hybridization may enhance offspring survival.

As further evidence that hybridization may be beneficial for *S. bombifrons* females, hybrid offspring of *S. bombifrons* females ("BM" tadpoles) developed significantly faster than did pure *S. bombifrons* tadpoles ("BB" tadpoles) when reared in the lab for 16 days (*18*) [mean difference in Gosner developmental stage, BB – BM = –0.75 ± 0.28 (SEM), $t_{97} = -2.67$, $P = 0.009$]. Additionally, for tadpoles reared in naturally drying artificial pools in the field (*14*, *18*), the likelihood that all tadpoles metamorphosed in a given replicate was higher for BM tadpoles (likelihood ratio $\chi_1^2 = 8.15$, $P = 0.004$) and increased with maternal condition ($\chi_1^2 = 4.70$, $P = 0.03$). Similarly, the proportion of tadpoles in a replicate that metamorphosed (*18*) was higher for BM tadpoles ($F_{1,53} = 11.76$, $P = 0.001$) and increased with maternal condition ($F_{1,53} = 3.98$, $P = 0.05$).

Hybridization by *S. bombifrons* females therefore results in a trade-off: Hybrid offspring may have lower fertility and fecundity, but they can develop faster than pure *S. bombifrons* offspring and may therefore be more likely to escape a drying pool. Consequently, the fitness effects of hybridization depend on the habitat in which offspring develop. Because pond duration depends largely on initial pond size and depth [deeper ponds generally outlast shallow ones (*17*)], in deep (long-lasting) ponds, pure *S. bombifrons* offspring can metamorphose before the ponds dry (*14*). Thus, in such ponds, *S. bombifrons* females would have higher fitness by mating with conspecifics. In contrast, in shallow (rapidly drying) ponds, hybridization may be beneficial for *S. bombifrons* females because hybrids are more likely than pure *S. bombifrons* offspring to escape and therefore to survive. Furthermore, a given pond's depth (and longevity) can vary dramatically with the amount of yearly rainfall (Fig. 1, A and B). Thus, because *S. bombifrons* females may encounter year-to-year variation in pond longevity, they may facultatively adjust their choice for conspecific versus heterospecific mates, depending on the depth of their breeding pond.

To evaluate this hypothesis, I tested two predictions by performing controlled mate-choice tests in the lab (*18*). First, I predicted that *S. bombifrons* females would more likely choose *S. multiplicata* males in shallow ponds than in deep ponds. Second, because maternal condition predicts the likelihood that offspring will metamorphose, I predicted that *S. bombifrons* females in relatively poor condition would be more apt than those in good condition to alter their choice for conspecifics depending on water level.

S. bombifrons females were presented with calls of conspecific versus heterospecific (*S. multiplicata*) males under conditions simulating a deep (long-duration) pond versus a shallow (short-duration) pond (*18*). When females were tested three times in a deep pool (*18*), they showed a significant preference for conspecific calls versus heterospecific calls (Wilcoxon signed rank = 245,

Department of Biology, Campus Box 3280, Coker Hall, University of North Carolina, Chapel Hill, NC 27599, USA. E-mail: kpfennig@email.unc.edu

Downloaded from www.sciencemag.org on November 14, 2007